This is a preprint, the final version is subject to change, of the American Mineralogist (MSA)
Cite as Authors (Year) Title. American Mineralogist, in press.
(DOI will not work until issue is live.) DOI: http://dx.doi.org/10.2138/am-2016-5531

Revision 2 – May 3, 2016

Comparison of Isoelectric Points of Single-Crystal and Polycrystalline α-Al_2O_3 and α-Fe_2O_3 Surfaces

Yingge Wang[a], Per Persson[b], F. Marc Michel[a, c, +], and Gordon E. Brown, Jr.[a, c*]

[a] *Surface & Aqueous Geochemistry Group, Department of Geological Sciences, School of Earth, Energy, and Environmental Sciences, Stanford University, Stanford, CA 94305-2115, USA*

[b] *Centre for Environmental and Climate Research & Department of Biology, Lund University, SE-22362, Lund, Sweden*

[c] *Department of Photon Science and Stanford Synchrotron Radiation Lightsource, SLAC National Accelerator Laboratory, MS 69, 2575 Sand Hill Road, Menlo Park, CA 94025, USA*

Submitted to *American Mineralogist* on August 13, 2015
Resubmitted to *American Mineralogist* (following reviews and revisions) on May 3, 2016

*Corresponding author address: Department of Geological Sciences, Stanford University, Stanford, CA 94305-2115, USA; Tel.: +1 650-723-9168, fax: +1 650-725-2199
Email: gordon.brown@stanford.edu

[+] Present address: Dept. of Geosciences, Virginia Tech, Blacksburg, VA 24061, USA

This is a preprint, the final version is subject to change, of the American Mineralogist (MSA)
Cite as Authors (Year) Title. American Mineralogist, in press.
(DOI will not work until issue is live.) DOI: http://dx.doi.org/10.2138/am-2016-5531
Revision 2 – May 3, 2016

Abstract

The surface charging behavior as a function of pH and isoelectric points (IEPs) of single-crystal α-Al_2O_3 (0001) and (1-102) and α-Fe_2O_3 (0001) were determined by streaming potential measurements using an electrokinetic analyzer. The IEPs of α-Al_2O_3 (0001) and (1-102) and α-Fe_2O_3 (0001) were found to be 4.5, 5.1, and 6.5, respectively. These IEP values for oriented single crystals of α-Al_2O_3 are in good agreement with literature values, whereas the new IEP value for α-Fe_2O_3 (0001) is significantly lower than four reported values (IEP = 8 to 8.5) for single-crystal α-Fe_2O_3 (0001) (Eggleston and Jordan, 1998; Zarzycki et al., 2011; Chatman et al., 2013; Lützenkirchen et al., 2013) and significantly higher than one (IEP = 4) recently measured by Lützenkirchen et al. (2015) on a fresh α-Fe_2O_3 (0001) surface. Most of the single-crystal IEP values measured recently are lower than IEP values reported for polycrystalline α-Al_2O_3 and α-Fe_2O_3, which are generally in the pH range of 8 to 10. Calculations of the IEP values based on estimated K_a values of α-Fe_2O_3 and α-Al_2O_3 surfaces in contact with water as a function of defect type and concentration suggest that highly reactive surface defect sites (primarily singly coordinated aquo groups) on the Fe- and Al-oxide powders are possibly a major source of the surface charge differences between polycrystalline samples and their oriented single-crystal counterparts studied here. The results of this study provide a better understanding of the surface charging behavior of Fe and Al-oxides, which is essential for predicting complex processes such as metal-ion sorption occurring at mineral/water interfaces.

Keywords: isoelectric point (IEP), pH point of zero charge (pH_{PZC}), Fe- and Al-oxide, single crystal, polycrystalline, surface defects

INTRODUCTION

Oxides and oxyhydroxides of iron and aluminum, as well as several other common metals (e.g., Mn), are among the most reactive mineral phases in the natural environment (e.g., Brown et al., 1999; Stipp et al., 2002). Due to their high surface reactivities and large surface areas, these metal-(oxyhydr)oxides often serve as natural sorbents of aqueous metal and metalloid species (e.g., Goldberg et al., 1996; Cornell and Schwertmann, 2003) as well as natural organic molecules (e.g., Gu et al., 1996; Nordin et al., 1998) and thus are important in controlling their transport and environmental fate. In addition to their importance in environmental chemistry, synthetic Fe- and Al-(oxyhydr)oxides are manufactured in bulk for use in a wide variety of technological and industrial applications. Synthetic polycrystalline α-Al_2O_3 (corundum) and α-Fe_2O_3 (hematite) are also commonly used in the production of ceramics and paints, as well as catalysts and catalyst supports (Yang and Troczynski, 1999; Avgouropoulos et al., 2002; Weiss and Ranke, 2002; Kershner et al., 2004; Franks and Gan, 2007). Moreover, synthetic α-Al_2O_3 single crystals and epitaxial α-Fe_2O_3 thin films have important applications in the optical and electrochemical industries (Weiss and Ranke, 2002).

Understanding the factors that control the surface reactivity of Fe- and Al-(oxyhydr)oxides in natural and technological systems is an important goal in all of the above applications. Key factors include the structure, composition, and concentration of reactive surface sites/functional groups and their effect on charging behavior. Surface charge is an important property of metal oxide/water interfaces that affects surface reactivity and is essential for determining or predicting many interfacial phenomena such as the stability of particles/colloids and the sorption behavior of trace elements and organic films on metal-oxide surfaces (Parks, 1965; Venema et al., 1998; Franks and Lange, 1999; Franks and Gan, 2007;

Kosmulski, 2009a). Surface charge has recently been implicated as an important variable in the toxicity of manufactured silver nanoparticles with various organic coatings, with more positively charged nanoparticle surfaces being more toxic to biological organisms than negatively charged nanoparticle surfaces (El Badawy et al., 2011). Surface charge is generally defined relative to the pH point of zero charge (pH_{PZC}), which refers to the pH value at which the electrical charge on the surface is zero (Sposito, 1984). Other types of pH_{PZCs} are reported in the literature and discussed by Sposito (1984). If there is no specific adsorption of ions on the surface, the value of pH_{PZC} determined by potentiometric titration matches the isoelectric point (IEP) determined by electrokinetic measurements (Sposito, 1984; Kosmulski, 2001). This is often the case for a "pristine surface" such as pure metal oxides in water or aqueous solutions with background electrolytes. In this paper, pH_{PZC} and IEP values should be considered as interchangeable because we measured the surface charge using 0.01 M NaCl as the background electrolyte, which is generally considered to be a non-specific, indifferent adsorption medium.

The hydrated surfaces of Fe- and Al-(oxyhydr)oxides have several different functional groups [e.g., $(Me)OH_2^{+0.5}$, $(Me)_2OH_2^{+1.0}$, $(Me)_2OH$, $(Me)_3OH^{+0.5}$, where Me represents Al^{3+} or Fe^{3+}] (Hiemstra et al., 1989; Venema et al., 1998; Eng et al., 2000; Trainor et al., 2002, 2004; Tanwar et al., 2007) and show pH-dependent variation in surface charges. For polycrystalline and nanocrystalline Fe- and Al-(oxyhydr)oxide samples, surface charge is typically positive at neutral pH. At pH values above or below the pH_{PZC}, the surface charge is dominantly negative or positive, respectively (Parks, 1965; Sposito, 1984; Franks and Lange, 1999; Franks and Gan, 2007). Numerous studies of polycrystalline and nanocrystalline α-Al_2O_3 consistently report IEP values in the range of 8 to 10 (Parks, 1965; Kosmulski, 2001, 2004, 2006, 2009a, 2009b, 2009c). In the case of polycrystalline α-Fe_2O_3, the IEP values for most synthetic hematite particles are

found to be in the range of 8 to 9, whereas the IEP values of natural hematite in polycrystalline (powdered) form are found to be somewhat lower (6 to 7) (Parks, 1965; Kosmulski, 2001, 2004, 2006, 2009a, 2009b). Such differences between synthetic and natural hematite may result from different sample origins and could be due, in part, to the effects of compositional impurities in the natural samples. Sverjensky (1994) modified crystal chemical and electrostatic models of the IEP by considering electrostatic solvation theory and predicted the IEP values of α-Fe_2O_3 and α-Al_2O_3 to be 8.47 and 9.37, respectively, which are in good agreement with measured IEP values for polycrystalline (powdered) samples (Parks, 1965; Kosmulski, 2001, 2004, 2006, 2009a, 2009b, 2009c).

In contrast to polycrystalline samples, oriented single-crystal α-Al_2O_3 (0001) and (1-102) surfaces have significantly lower IEP values in the pH range of 4-6 (Larson et al., 1997; Franks and Meagher, 2003; Fitts et al., 2005; Franks and Gan, 2007; Zhang et al., 2008; Lützenkirchen et al., 2010). The predicted IEP value for α-Al_2O_3 (9.37) based on the model of Sverjensky (1994) is significantly higher than measured values reported for single-crystal surfaces. The difference between the IEPs of single-crystal and powdered, polycrystalline forms of α-Al_2O_3 has been a subject of debate over the last two decades (Sverjensky, 1994; Franks and Meagher, 2003; Fitts et al., 2005; Franks and Gan, 2007; Zhang et al., 2008; Lützenkirchen et al., 2010).

Several studies have reported IEP values (ranging from 7 to 8.5) for single-crystal α-Fe_2O_3 (0001) surfaces (Eggleston and Jordan, 1998; Zarzycki et al., 2011; Chatman et al., 2013; Lützenkirchen et al., 2013), which are similar to IEP values reported for polycrystalline (powdered) hematite powders. More recently Lützenkirchen et al. (2015) reported a much lower IEP value (~4) for a fresh α-Fe_2O_3 (0001) surface and found that aging of this surface in 1mM NaCl solution resulted in an increase in IEP from 4 to about 9, which they attributed to a change

126 in surface structure and surface roughening caused by exposure of the α-Fe_2O_3 (0001) surface to
127 the electrolyte solution. As is the case for α-Al_2O_3, the IEP predicted for α-Fe_2O_3 using the
128 Sverjensky (1994) model (8.47) is higher than measured values for single crystal α-Fe_2O_3
129 surfaces.

130 In general, the variation in reported IEPs for α-Al_2O_3 and α-Fe_2O_3 (Parks, 1965; Loaec et
131 al., 1997; Wightman and Fein, 2001; Hizal et al., 2009) is likely due to differences in the source
132 (i.e. commercially available, laboratory synthesized, natural), the specific form of the material
133 (single crystal vs. polycrystalline (powdered), and/or different morphologies), and sample
134 preparation methods (Franks and Gan, 2007), including the effects of aging α-Fe_2O_3 surfaces
135 (Lützenkirchen et al., 2013; 2015). In the case of polycrystalline samples, particle size may also
136 play an important role, in particular for particles in the nanometer-sized regime (Vayssieres,
137 2009). The methods used for determining surface charge, as well as the specific conditions under
138 which the experiments were conducted, must also be considered.

139 A number of methods can be used to experimentally determine the IEPs or pH_{PZCs} for
140 polycrystalline samples, including classic electrokinetic measurements, potentiometric titration,
141 sedimentary potential, and acoustic methods (Parks, 1965; Larson et al., 1997; Kosmulski, 2001;
142 Stack et al., 2001; Franks and Meagher, 2003; Kosmulski, 2004, 2006; Franks and Gan, 2007;
143 Zhang et al., 2008; Kosmulski, 2009b). For near atomically flat surfaces such as oriented single
144 crystals, streaming potential measurements and more recently developed surface-sensitive
145 methods, such as atomic force microscopy (AFM) and non-linear optical surface spectroscopies
146 such as second harmonic generation (SHG) and sum-frequency vibrational spectroscopy (SFVS),
147 and cyclic potentiometric titration in which the single-crystal surface serves as an electrode
148 (referred to as the single-crystal electrode (SCrE) method), can be used to determine IEP values

(Larson et al., 1997; Stack et al., 2001; Franks and Meagher, 2003; Fitts et al., 2005; Zhang et al., 2008; Lützenkirchen et al., 2010; Zarzycki et al., 2011; Chatman et al., 2013; Lützenkirchen et al., 2015). In the present study we used streaming potential measurements to experimentally determine the surface charges of oriented single crystals of synthetic α-Al_2O_3 and natural α-Fe_2O_3.

Here we report the isoelectric points of oriented single-crystal surfaces of synthetic α-Al_2O_3 (0001) and (1-102) and natural α-Fe_2O_3 (0001) and compare the results with IEPs reported previously for oriented single-crystal α-Al_2O_3 and α-Fe_2O_3 surfaces and polycrystalline (powdered) samples of α-Al_2O_3 and α-Fe_2O_3 as well as with predicted IEP values. The various factors affecting the surface charging behavior of metal oxides are also discussed. In addition, we present simple model calculations of the IEP values of these metal oxides as a function of pH, based on estimated K_a values and surface structures determined experimentally in an earlier crystal truncation rod (CTR) diffraction study of the hydrated α-Al_2O_3 (0001) (Eng et al., 2000), α-Al_2O_3 (1-102) (Trainor et al., 2002), and α-Fe_2O_3 (0001) (Trainor et al., 2004) surfaces. Our surface charging measurements were made on single crystal samples from the same sources and prepared in the same way as the surfaces used in the CTR measurements of α-Al_2O_3 (0001) and (1-102) and α-Fe_2O_3 (0001) surfaces. As a consequence, the average structures of these hydrated surfaces are reasonably well known rather than based on the assumptions that the surface structures are simple terminations of the bulk structures without relaxation or that water does not affect the surface structure of the solids. In addition, the surfaces were characterized using AFM and XPS measurements, which provide quantitative information on step densities and coverage by adventitious carbon, respectively. Comparison of these calculated values with measured IEPs suggests that IEPs are very sensitive to defect concentrations on the metal-oxide surfaces,

consistent with earlier suggestions for the surface charging behavior of single-crystal α-$Al(OH)_3$ (001) and (100) and α-Al_2O_3 (0001) (Franks and Gan, 2007) and of iron-(oxyhydr)oxides (Venema et al., 1998; Zarzycki et al., 2011; Chatman et al., 2013; Lützenkirchen et al., 2013; 2015).

EXPERIMENTAL METHODS

Sample preparation

The metal-oxide substrates used in these experiments are commercially available, highly polished 2-inch diameter α-Al_2O_3 (0001) and (1-102) single crystals (Saint-Gobain Crystals & Detectors Co.) and natural hematite (α-Fe_2O_3 - variety specularite) single crystals from Bahia, Brazil with well-developed (0001) faces. The α-Fe_2O_3 crystals were prepared using a chemical-mechanical polishing (CMP) procedure that results in surfaces of sufficient quality (surface roughness less than 5Å rms) for crystal truncation rod (CTR) diffraction studies (Eng et al., 2000; Trainor et al., 2002, 2004; Tanwar et al., 2007). Prior to the streaming potential measurements, the α-Fe_2O_3 (0001) single crystals were initially rinsed with acetone, washed in $10^{-3.5}$ M sodium hydroxide for 20 minutes, and finally washed in 10^{-2} M nitric acid for one hour. Each chemical washing step was followed by multiple rinses with MilliQ water. The 2-inch diameter commercial α-Al_2O_3 crystals were cut into 2" x 1" rectangular pieces, washed as described above, and then baked at 350 °C for 4 h to minimize excess carbon on the surfaces. The cleaning procedure was repeated as necessary until the adventitious carbon content at the crystal surfaces was less than ~10% of a monolayer and there were no detectable trace elements, including silicon (<0.1%), as determined by x-ray photoelectron spectroscopy (XPS) (Surface Science S-Probe, monochromatic Al K_α radiation). Atomic force microscopy (AFM) (Veeco

Multimode Scanning probe microscope) imaging was conducted on the α-Al_2O_3 and α-Fe_2O_3 surfaces. In addition, x-ray reflectivity data for the three crystal surfaces examined here were collected on a PANalytical X'Pert 2 diffractometer in the Geballe Laboratory for Advanced Materials at Stanford University.

Streaming potential measurements of single crystal surfaces

Streaming potential was measured for the three polished single-crystal crystal surfaces using an electrokinetic analyzer (EKA) equipped with an asymmetric clamping cell with a platinum electrode on each end (Anton Paar, Graz, Austria). The EKA includes an automatic pH titrator, external pH and conductivity electrodes, asymmetric flow cell, and computer-based control system. During each measurement, the sample was placed against a poly(methyl methacrylate) (PMMA) channel reference plate in the flow cell. The pH, conductivity, and electrode potential were recorded as a function of pH ranging from 3.0 to 9.0 at room temperature, with a 0.01 M aqueous solution of sodium chloride as the background electrolyte. An automatic pH titrator was used to slowly increase the pH of the electrolyte solution from 3.0 to 9.0 by adding aliquots of 1 N sodium hydroxide. The electrolyte solution was degassed before each analysis and purged continuously using ultra-pure N_2 gas to minimize carbonate contamination during the measurement of streaming potential. The flow directions were alternated for each measurement and averaged to account for any deviations from the geometry of the flow cell. The pH, conductivity, and electrode potential were calibrated before each measurement. Six measurements were performed at a single pH point in alternating flow directions, and the equilibration time for a single-point measurement was at least 15 minutes.

Streaming potential is generated when an electrolyte solution is forced by hydraulic pressure to flow across the channel between two plates. It can be computed from the Helmholtz-

Smoluchowski equation using the Fairbrother and Mastin substitution (Fa et al., 2005) as incorporated in Eq. 1:

$$\zeta = \frac{E_s}{\Delta P}\frac{\eta}{\varepsilon\varepsilon_0}k_s \quad [1]$$

where ζ is the streaming potential, E_s is the induced streaming potential, ΔP is the hydraulic pressure, η is the liquid viscosity, ε is the liquid permittivity, ε_o is the permittivity in vacuum, and k_s is the specific conductance of the electrolyte solution. The streaming potential of the sample is calculated from the measured streaming potential of the sample, $\zeta_{measured}$, and PMMA reference, ζ_{PMMA}, using Eq. 2 (Fa et al., 2005):

$$\zeta = 2\zeta_{measured} - \zeta_{PMMA} \quad [2]$$

The single-crystal α-Al_2O_3 and α-Fe_2O_3 samples were cleaned using the CMP procedure (see section 2.1) and were stored in MilliQ water in polypropylene containers for 24 hr and rinsed with MilliQ water multiple times before mounting them in the cell. Surface contamination by carbon and silica was evaluated before and after each measurement by XPS. The EKA system was cleaned by rinsing with 2 L each of MilliQ water, 1 mM NaOH, MilliQ water, 1 mM HCl, and MilliQ water in this order without recirculation. Air bubbles were also removed from the apparatus during the rinsing cycle. After mounting each sample, the system was flushed with 2 L of 10 mM NaCl at pH 3, and a flow check was performed to insure reproducible pressure readings before the measurements. This acid treatment should have removed any remaining carbonate/bicarbonate contamination on the single-crystal surfaces. The streaming potential of the PMMA reference plate was measured before and after each sample measurement.

RESULTS AND DISCUSSION

Surface charge characterization of single-crystal α-Al_2O_3 and α-Fe_2O_3 surfaces

Streaming potentials as a function of pH for the three single-crystal substrates examined in this study are shown in Figure 1. The error bars include the average standard deviation for 6 measurements at each point plus the average standard deviation from the PMMA reference plate measurements. Surface charge for all three substrates decreased as pH was increased from 3 to 9 (in steps of ~ 0.25 pH units). The IEPs of α-Al_2O_3 (0001) and (1-102) and α-Fe_2O_3 (0001) are 4.5, 5.1, and 6.5, respectively (the pH crossing points at zero streaming potential).

Because XPS analyses of the surfaces showed only small amounts of adventitious carbon (<10%) and silica (<0.1%) contamination after the streaming potential measurements, surface charge modifications from carbonate and/or silica contamination should not have been significant. Note also that XPS measurements were conducted *ex situ,* and a large part of the detected adventitious carbon is likely to have formed after the streaming potential measurements, especially considering the experimental procedure involving acid flushing as described above.

As shown in Table 1, the IEP values for α-Al_2O_3 (0001) and (1-102) are in good agreement with literature values (Veeramasuneni et al., 1996; Larson et al., 1997; Stack et al., 2001; Franks and Meagher, 2003; Tulpar et al., 2005; Franks and Gan, 2007; Lützenkirchen et al., 2010), except for two studies where the surfaces were plasma cleaned, which resulted in significantly higher IEP values of 8.5 and 9.3 for α-Al_2O_3 (0001) (Veeramasuneni et al., 1996; Tulpar et al., 2005). The IEP value determined for α-Fe_2O_3 (0001) in the present study differs from that of Eggleston and Jordan (1998) who used scanning force microscopy to determine the IEP of α-Fe_2O_3 (0001) and found IEP values ranging from 8 to 8.5 depending on the types of probe tips and electrolyte solutions used (Table 1). However, no detailed surface properties or

cleaning procedures were reported by Eggleston and Jordan (1998), although they noted that steps about 10 nm high were commonly found for a similarly prepared quartz single crystal. Thus, a higher surface roughness might be expected for the single-crystal hematite used in this earlier study because hematite has a lower hardness than that of crystalline quartz (Eggleston and Jordan, 1998; Trainor et al., 2004).

The charging behavior of synthetic platy crystals of hematite with 40-60% of the (001) face present was also measured and modeled by Venema et al. (1998) using potentiometric titrations and a modified MUSIC model in which the Pauling bond valences were calculated as a function of predicted bond lengths. The resulting measured value of the pristine point of zero charge for the platy hematite crystals is about 9.4, which is significantly higher than the value we report here (6.5). We attribute this difference, in part, to the presence of different faces on the synthetic crystals used in the measurements by Venema et al., particularly (110) faces. In addition, no information was provided by these authors on the actual structure or composition of the surfaces of the crystals used. For modeling purposes, Venema et al. found that a mixture of 50% (001) and 50% (110) faces and the assumption of dominantly singly coordinated surface groups on the (001) surface and equal proportions of singly, doubly, and triply coordinated oxo, hydroxo, or aquo groups, respectively, on the (110) surface gave a reasonable match with the measured charging behavior.

Zarzycki et al. (2011) reported a new determination of the pH_{PZC} of a natural hematite (0001) surface using the SCrE cyclic potentiometry method in which hematite served as an electrode. The pH_{PZC} value they obtained (8.0) is similar to that measured by Eggleston and Jordan (1998) for single-crystal hematite and that measured for powdered hematite, but it differs from the IEP value for the α-Fe_2O_3 (0001) surface in the present study (6.5). One significant

289 difference between the Zarzycki et al. (2011) study and ours involves sample preparation.
290 Whereas Zarzycki et al. prepared their hematite (0001) surface by sawing a natural sample
291 parallel to the (0001) plane and then annealing the sample at 1100°C, which is now thought to
292 change the surface structure of hematite (0001) (Lützenkirchen et al., 2015), we prepared our
293 hematite (0001) and α-Al_2O_3 (0001) and (1-102) surfaces by a chemical-mechanical polishing
294 procedure documented in Trainor et al. (2002, 2004) and Tanwar et al. (2007). This procedure
295 resulted in a hematite (0001) surface with an rms roughness of 2.8 ± 0.6Å and an α-Al_2O_3 (0001)
296 surface with an rms roughness of 2.5 ± 0.6 Å as measured by AFM (Figures 2a and 2b), with few
297 resolvable steps in the 5μm x 5μm AFM images. These AFM roughnesses are consistent with
298 those determined by fitting x-ray reflectivity data (data not shown). In contrast, the 10μm x
299 10μm AFM image of the hematite (0001) surface examined by Zarzycki et al. (2011) before their
300 potentiometric titration measurements showed at least 12 step edges, with terraces between, the
301 widest of which was about 3 μm and the narrowest of which was < 0.5 μm. The significant
302 difference in surface roughness between our sample and the one used by Zarzycki et al. for
303 pH_{PZC} measurements helps explain the lower pH_{PZC} value for hematite (0001) obtained in the
304 present study vs. the Zarzycki et al. (2011) study. As discussed below, the greater surface defect
305 concentration of the hematite sample examined by Zarzycki et al. (2011) leads to a higher pH_{PZC}
306 value.

307 Three more recent studies of the surface charging behavior and IEP of α-Fe_2O_3 (0001)
308 were conducted by Chapman et al. (2013), Lützenkirchen et al. (2013), and Lützenkirchen et al.
309 (2015) using the SCrE cyclic potentiometric method. In the study by Chatman et al. (2013), a
310 PZC value of 8.35 was determined on a natural hematite sample prepared by sawing and
311 annealing at 1100°C, whereas in the study by Lützenkirchen et al. (2013) using natural hematite

312 samples prepared by chemical-mechanical polishing and cleaning followed by annealing at
313 1200^{o}C, the point of zero potential was determined to be 8.1 or 8.4, the latter value being
314 determined by applying the "common intersection point" (see Zarzycki and Preocanin, 2012).
315 Both of these studies used the SCrE cyclic potentiometry method to measure surface potentials.
316 However, similar charging behaviors were found for fresh and aged hematite samples using the
317 SCrE cyclic potentiometry method for the surface potential measurements performed in a more
318 recent study by Lützenkirchen et al. (2015), whereas their zeta-potential measurements (similar
319 to the streaming potential measurements used in this study) showed a dramatic difference
320 between the two samples (4 vs. 9). This suggests that the surface potential measurements and
321 IEP value determinations depend strongly on the methods used. Because aluminum oxide is an
322 electrical insulator, there are no available SCrE cyclic potentiometric studies of more extensively
323 investigated single-crystal aluminum-oxide surfaces in the literature for comparison with IEP
324 values determined using this method with other techniques.

325 In the streaming potential study by Lützenkirchen et al. (2015) an IEP value of about 4
326 was determined on a well-characterized fresh, natural hematite sample prepared by the same
327 chemical-mechanical polishing procedure used in the present study. This study also determined
328 the zeta potential value of an aged hematite surface coupled with AFM and crystal truncation rod
329 (CTR) diffraction measurements on surfaces with similar preparation histories. Surface
330 roughness as measured by AFM on the α-Fe_2O_3 (0001) sample studied by Lützenkirchen et al.
331 (2015) was about 1.2Å in air, about 4.2Å in water, and about 6Å in 1 mM KCl solution. The
332 CTR data for the fresh hematite (0001) surface were best fit with two different structural
333 domains, one (domain 1), referred to as the oxygen (or hydroxyl)-terminated surface, that
334 comprises about 44% of the surface and is terminated dominantly by doubly coordinated

hydroxo groups, and one (domain 2), referred to as the iron-terminated surface, that comprises about 56% of the surface and is terminated dominantly by separated $Fe(III)(O,OH)_6$ octahedra with three singly coordinated aquo groups in contact with the aqueous solution. No ordered water layer was required to fit the CTR data for the fresh hematite sample. AFM images of the fresh hematite surface suggest 10-30 nm diameter patches representing the two domains on the (0001) surface. CTR data for the aged hematite (0001) surface were also best fit by the same two types of structural domains, except that domain 1 increased to 68% of the total surface and domain 2 was reduced to 32% as a result of aging in aqueous solution. In addition, the best-fit structure included 20% of an ordered monolayer of water and the terminal Fe-O bond lengths are reduced relative to the fresh surface. Although the concentration of the singly coordinated surface groups decreased from aged to fresh samples, the increased reactivity of these functional groups on the aged sample is attributed to its dramatically elevated IEP value (9). Because our sample was hydrated for 24 hr before the steaming potential measurements, the IEP value we measured (6.5) lies in the intermediate range of their observed IEP shifts from fresh (4) to fully aged stage (9).

Differences between IEPs of α-Al_2O_3 and α-Fe_2O_3 single-crystal surfaces and powders

Figure 3a shows the distribution of IEP values of α-Al_2O_3 polycrystalline powders from various sources collected by different investigators. Various methods have been used to measure the IEPs of α-Al_2O_3 powders including the electrokinetic method, titration at a common interception point (cip), electroacoustic methods, and atomic force microscopy (AFM) (Parks, 1965; Kosmulski, 2001, 2004, 2006, 2009b). With the exception of a few studies, the reported IEP values of polycrystalline α-Al_2O_3 are generally in the pH range of 8 to 10. In comparison, the IEP values of α-Al_2O_3 (0001) and (1-102) single-crystal surfaces examined in this study and

359 others are much lower, and the difference are due, in part, to differences in the protonation states
360 and types of binding environments (i.e. surface functional groups) present on the surfaces of
361 powder vs. single-crystal samples (Fitts et al., 2005; Franks and Gan, 2007; Zhang et al., 2008).
362 Lützenkirchen et al. (2010) attributed the difference between the negative zeta potential of α-
363 Al_2O_3 (0001) single-crystal surfaces in the pH range 5-7 and the IEP prediction (5.4) by the
364 MUSIC model to enhanced auto-protolysis of interfacial water. In addition, they reviewed the
365 differences in charging behavior and IEPs on single-crystal α-Al_2O_3 (0001) observed using
366 several different methods.

367 Surface reactivities of Fe- and Al-oxides are expected to increase due to the presence of
368 point defects such as vacancies as well as the formation of step edges that are normally
369 associated with surface roughening (Liu et al., 1998). Both factors may affect the IEP values of
370 polycrystalline and single crystal samples (Stipp et al., 2002). Several studies have shown that
371 plasma treatment of the α-Al_2O_3 (0001) surface results in significantly higher IEP values relative
372 to untreated α-Al_2O_3 (0001) surfaces (Veeramasuneni et al., 1996; Tulpar et al., 2005; Franks
373 and Gan, 2007). In accordance with the preceding discussion, the increase in IEP from single
374 crystals to polycrystalline samples is attributed to surface roughening and the formation of
375 vacancy defects for the latter, which are expected to increase the fraction of singly coordinated
376 surface hydroxyl groups associated with cation vacancies. In contrast to oriented single crystals,
377 polycrystalline alumina exhibits a mixture of different crystal terminations, and the proportion of
378 each depends on morphology. Small particles are expected to have large surface defect densities
379 such as step edges and vacancies (Franks and Gan, 2007; Zhang et al., 2008). Accordingly, α-
380 Al_2O_3 in polycrystalline form is expected to have a high number of singly coordinated surface
381 aquo groups, which have pK_a values of 9 to 11 (Franks and Gan, 2007). This range is quite close

to most of the IEP values reported in the literature for polycrystalline alumina (Figure 3a). These results support the notion that singly coordinated surface functional groups resulting from the presence of surface defects on individual Al-oxide particles may be a major cause of the surface charge differences between the polycrystalline powders and the single-crystal counterparts studied here and reported elsewhere (Franks and Gan, 2007; Zhang et al., 2008).

The IEP values reported for polycrystalline α-Fe_2O_3 vary more widely (Figure 3b) (Parks, 1965; Kosmulski, 2001, 2004, 2006, 2009b) than those for polycrystalline α-Al_2O_3 (Figure 3a). In the case of compositionally pure synthetic α-Fe_2O_3 samples, the variation may be primarily attributable to different preparation methods, which yield a wide range of particle sizes and morphologies as shown in Table 3 (see section below on the effect of particle size on IEP).

Modeling the charging behavior of α-Al_2O_3 (0001) and (1-102) surfaces as a function of pH

When in contact with water, three types of surface functional groups for α-Al_2O_3 (singly coordinated aquo, doubly coordinated hydroxo, and triply coordinated oxo) (Fitts et al., 2005; Franks and Gan, 2007; Zhang et al., 2008) are thought to form protonated Al_nOH_x species characterized by specific K_a values (Table 2) (Hiemstra et al., 1989; Fitts et al., 2005; Franks and Gan, 2007; Zhang et al., 2008). As discussed earlier, the hydrated α-Al_2O_3 (0001) surface has dominantly doubly coordinated Al_2OH^0 surface functional groups (Eng et al., 2000) that are characterized by the following acid-base equilibrium constants (Hiemstra et al., 1989):

$$K_1 = [Al_2O^-][H^+]/[Al_2OH^0] \quad [3]$$

$$K_2 = [Al_2OH^0][H^+]/[Al_2OH_2^+] \quad [4]$$

By rearranging Equations [3] and [4] and equating $[Al_2O^-] = [Al_2(OH)_2^+]$, the theoretical IEP value can be calculated as the average of equilibrium constants for specific (hydr)oxo surface functional groups (Fitts et al., 2005; Zhang et al., 2008), and a theoretical IEP value of ~5.4

408 ((pK_1+pK_2)/2) is obtained for the α-Al_2O_3 (0001) surface (Hiemstra et al., 1989). This IEP is
409 determined by two pK_a values separated by more than 13 units, and at or around pH 5.4 the
410 surface speciation is completely dominated by neutral Al_2OH groups, which implies a very low
411 surface charge density in the surface plane. Accordingly, the IEP of α-Al_2O_3 (0001) will be
412 sensitive to small amounts of charged defect sites, such as singly coordinated oxo (or hydroxo)
413 groups, which are present at step-edges, corners, and vacant surface sites (point defects). This
414 sensitivity is exemplified by the results of model calculations presented in Figure 4, which show
415 that even low concentrations of singly coordinated (hydr)oxo groups shift the IEP to
416 substantially higher values. Note, however, that the presence of these singly coordinated groups
417 may be partly balanced by other surface charging mechanisms as suggested by Lützenkirchen et
418 al. (2010). The sensitivity of calculated pH_{PZC} values of metal-oxide surfaces to the surface
419 structural model assumed has also been pointed out by Lützenkirchen et al. (2010) and Zarzycki
420 et al. (2011).

421 The variation of surface charge with pH was calculated as follows for the hydrated α-
422 Al_2O_3 (0001) surface, which has mainly doubly coordinated functional groups (Eng et al., 2000),
423 as expressed in equation [5].

424 $$[Al_2OH]_{tot} = [Al_2OH_2^+] + [Al_2OH] + [Al_2O^-] \quad [5]$$
425
426 At low pH equation [5] can be approximated by
427
428 $$[Al_2OH]_{tot} = [Al_2OH_2^+] + [Al_2OH] \quad [6]$$
429
430 Whereas at high pH equation [5] can be approximated by
431
432 $$[Al_2OH]_{tot} = [Al_2OH] + [Al_2O^-] \quad [7]$$
433

434 From the acid-base equilibria, the following equations are obtained, with K_a values for the
435 different surface functional groups from the classical MUSIC model (Hiemstra et al., 1989).

$$[Al_2OH][H^+]/[Al_2OH_2^+] = K_a \quad [8]$$

$$[Al_2O^-][H^+]/[Al_2OH] = K_a \quad [9]$$

Combining equations [6] and [8] yields

$$[Al_2OH_2^+] = [Al_2OH]_{tot}[H^+]/(K_a + [H^+]) \quad [10]$$

and combining equations [7] and [9] yields

$$[Al_2O^-] = [Al_2OH]_{tot}K_a/(K_a + [H^+]) \quad [11]$$

Summing equations [10] and [11] gives the surface charge generated by the doubly coordinated (hydr)oxo sites.

One can also estimate the contribution to surface charge as a function of pH of singly coordinated defect sites on the α-Al_2O_3 (0001) surface, which is given by ½($[AlOH_2^{+0.5}]$ + $[AlOH^{-0.5}]$) and can be calculated as follows:

$$[AlOH]_{tot} = [AlOH_2^{+0.5}] + [AlOH^{-0.5}] \quad [12]$$

$$[AlOH^{-0.5}][H^+]/[AlOH_2^{+0.5}] = K_a \quad [13]$$

Combining equations [12] and [13] and solving for $[AlOH_2^{+0.5}]$ yields

$$[AlOH_2^{+0.5}] = [AlOH]_{tot}[H^+]/(K_a + [H^+]) \quad [14]$$

Combining equations [12] and [13] and solving for $[AlOH^{-0.5}]$ yields

$$[AlOH^{-0.5}] = [AlOH]_{tot}K_a/(K_a + [H^+]) \quad [15]$$

Summation of equations [10], -[11], ½[14], and -½[15] gives the surface charge of the α-Al_2O_3 (0001) surface as a function of pH, including singly coordinated surface defect sites.

This modeling highlights the difficulty in experimental determination of the IEP value of pristine α-Al_2O_3(0001) assuming that no other mechanism is controlling the surface charging behavior. Because hydrated α-Al_2O_3(1-102) has, in addition to $Al_2(OH)^0$, approximately equal amounts of $Al(OH)^{-0.5}$ and $Al_3(OH)^{0.5}$ functional groups (Trainor et al., 2002), its theoretical IEP

should be higher than that of the (0001) surface (see Table 2), which is consistent with the trend of the measured values in the present study. However, due to the sensitivity of IEP to the precise distribution of surface functional groups and the uncertainties of reported K_a values, comparisons between theoretical and measured IEPs should be made with caution and only be interpreted in a qualitative sense.

Modeling the charging behavior of the α-Fe_2O_3 (0001) surface as a function of pH

Because the hydrated α-Fe_2O_3 (0001) surface has approximately equal amounts of the three functional groups, based on a crystal truncation rod x-ray diffraction study (Trainor et al., 2004), the theoretical IEP will mainly be determined by pK_a($Fe_3OH^{+0.5}$) and pK_a($FeOH_2^{+0.5}$) (see Table 2). Assuming equal amounts of the three surface groups, one can estimate the IEP values of the hydrated α-Fe_2O_3 (0001) surface as follows. By analogy with the equations for α-Al_2O_3 given above, the surface charge generated by the doubly coordinated sites on the hydrated α-Fe_2O_3 (0001) surface is given by

$$[Fe_2OH_2^+] = [Fe_2OH]_{tot}[H^+]/(K_a + [H^+]) \quad [16]$$

and

$$[Fe_2O^-] = [Fe_2OH]_{tot}K_a/(K_a + [H^+]) \quad [17]$$

The contribution to surface charge of singly coordinated surface sites is given by

$$[FeOH_2^{+0.5}] = [FeOH]_{tot}[H^+]/(K_a + [H^+]) \quad [18]$$

$$[FeOH^{-0.5}] = [FeOH]_{tot}K_a/(K_a + [H^+]) \quad [19]$$

and the contribution of triply coordinated surface sites is given by

$$[Fe_3OH^{+0.5}] = [Fe_3OH]_{tot}[H^+]/(K_a + [H^+]) \quad [20]$$

$$[Fe_3O^{-0.5}] = [Fe_3OH]_{tot}K_a/(K_a + [H^+]) \quad [21]$$

Summing equations [16], [17], ½[18], ½[19], ½[20] gives the total charge of the hydrated α-Fe_2O_3 (0001) surface as a function of pH.

Acid/base reactions similar to those occurring at various surface functional groups on hydrated α-Al_2O_3 surfaces have been proposed for hydrated α-Fe_2O_3 surfaces. These Fe_nOH functional groups include singly coordinated $FeOH^{-0.5}$, doubly coordinated Fe_2OH^0, and triply coordinated $Fe_3OH^{0.5}$ (Hiemstra et al., 1989; Venema et al., 1998; Trainor et al., 2004; Tanwar et al., 2007). The pK_a values of these sites were predicted by Hiemstra et al. (1989) using the "classical MUSIC model" as shown in Table 2 (Hiemstra et al., 1989; Venema et al., 1998).

The predicted IEP value (~7.2) of the hydrated α-Fe_2O_3 (0001) surface with a 2.0:2.0:2.0 ratio of singly to doubly to triply coordinated surface functional groups is higher than that measured in this study (6.5) as shown in Figure 5. However, Figure 5 also shows that the predicted IEP value is sensitive to the distribution of surface functional groups, which makes comparison with experimental values difficult. Venema et al. (1998) also predicted pristine point of zero charge (PPZC) values for hematite (0001) surfaces using a similar approach and concluded that PPZC values are high (>9.5) when the fraction of singly coordinated surface groups is high and low (<5) when the fraction of singly coordinated surface groups is low. Although the K_a values used in these model calculations have not been fully verified for different metal oxide surfaces due to variations in surface structure and composition, which are often poorly known, this approach provides a potential explanation for the relatively large differences between the IEP values measured for polycrystalline (powdered) and single-crystal α-Fe_2O_3.

Most of the α-Fe_2O_3 polycrystalline powders studied to date have IEP values of 8 to 9 (Figure 3b), which are significantly higher than the IEP of hydrated single-crystal α-Fe_2O_3(0001) obtained herein. This difference is consistent with the idea that singly coordinated Fe-OH_x

functional groups are expected to be more prevalent on surfaces of polycrystalline powders, which results in increasing IEP values as indicated by the K_a values (Venema et al., 1998). However, because the surface structures (functional group types and densities) and morphologies of particles in various powdered samples are not well known, especially for samples used in IEP measurements reported in the literature, it is not possible to rationalize the diverse IEP values for these powdered samples. This modeling also helps explain the significantly higher IEP value for hematite(0001) determined by Zarzycki et al. (2011); their hematite sample had more step-edges than our hematite (0001) sample.

Effect of particle size on IEP values

The IEP values of synthetic α-Fe_2O_3 particles, with sizes ranging from ~ 75 nm to 5 μm, vary from 10 to 6.5, respectively (Table 3). The samples in these studies were created under controlled conditions, and the size, morphology, and specific surface area of the particles are reported, which allows for a reasonable comparison of different studies. As suggested by the data reported in Table 3, a rough correlation exists between particle size and IEP values, with smaller particles exhibiting higher IEP values than larger particles. More data, especially for particles in the 1000 to 5000 nm size range, are needed to confirm or refute this proposed correlation of increasing IEP with decreasing particle size.

This suggested trend is consistent with that found in a study of pH_{PZC} variations of maghemite (γ-Fe_2O_3) nanoparticles of different sizes by Vayssieres (2009). He found that pH_{PZC} values increased from 6.3 to 8.4 as nanoparticle size decreased from 12.0 nm to 3.5 nm and attributed this increase to increased curvature of the nanoparticle surface with decreasing size, leading to a decrease in electrostatic repulsion between charged surface sites at the

548 nanoparticle/aqueous solution interface and an increase in the number of charged surface sites
549 (Vayssieres, 2009).

550 Vayssieres (2009) hypothesized that in the case of a metal-oxide system with negative
551 surface charge (i.e. pH > pH_{PZC}), this decrease in electrostatic repulsion between surface sites
552 with decreasing nanoparticle size could lead to an increase in charged surface sites and to
553 desorption of more protons at the same pH for smaller particles, and *"consequently the surface*
554 *chemistry will change accordingly and the acidity of the surface will decrease (the basicity will*
555 *increase), and thus the PZC will increase."* We hypothesize that the number of singly
556 coordinated (hydr)oxo groups should increase with decreasing particle size, resulting in an
557 increase in pH_{PZC} with decreasing particle size. In contrast, a recent study by Ridley et al. (2013)
558 suggests that nanoparticles do not necessarily have different PZC values than their larger
559 counterparts.

560
561 **Other factors affecting surface charging behavior of metal oxides**

562 In addition to size, particle morphology is also expected to impact IEP due to the
563 presence of different proportions of singly, doubly, and triply coordinated surface groups on
564 different surfaces of the same particle (see, e.g., Venema et al., 1998). However, a systematic
565 IEP study of well characterized α-Fe_2O_3 particles over a broad range of particle sizes and
566 morphologies using similar preparation protocols and the same method for IEP measurements is
567 needed to draw further conclusions about these factors. The measured IEP values of natural
568 polycrystalline α-Fe_2O_3 samples are generally lower than those of their synthetic counterparts,
569 and the deviation may also be attributable to a combination of variable particle size and
570 morphology effects (Parks, 1965; Kosmulski, 2001, 2004, 2006, 2009b). Similar to α-Al_2O_3, the
571 presence of various faces and defects on polycrystalline α-Fe_2O_3 samples could be a major

source of the observed differences between the IEP value for single-crystal α-Fe_2O_3(0001) measured in this study and IEP values reported in the literature.

At least one additional factor – surface composition – should have a major effect on the measured IEP values of metal oxides in contact with aqueous solutions (Franks and Gan, 2007). This is particularly true when a metal oxide surface has a partial monolayer or several effective monolayers of adventitious carbon, which can be in the form of various aliphatic hydrocarbons, carbonate ions, and functional groups such as carboxylates (Olefjord and Nylund, 1994; Barr and Seal, 1995; Miller et al., 2002; Bhargava et al., 2007). Such functional groups and carbonate ions are negatively charged and should have the effect of decreasing the IEP of the surface. In addition, natural mineral surfaces likely have bulk compositional impurities relative to their synthetic counterparts as well as partial coatings of natural organic matter that are rich in anionic functional groups (Gibbs, 1983; Chorover and Sposito, 1995; Mayer, 1999). Carbon *1s* x-ray photoelectron spectroscopy (XPS) analysis of the single-crystal samples used in the present study showed that the coverage of adventitious carbon was less than 10% of a monolayer on surfaces before and after streaming potential measurements, and the acid treatment of the surfaces prior to these measurements, as well as our sample cleaning and handling protocols, should have minimized the amount of adsorbed carbonate, other forms of adventitious carbon, and silica during the actual measurements. However, only a few published studies of the IEP values of single-crystal and polycrystalline forms of α-Al_2O_3 and α-Fe_2O_3 include XPS or Auger spectroscopy analyses of the samples (Stack et al., 2001; Franks and Meagher, 2003; Kershner et al., 2004), so it is not generally possible to estimate how significant this effect is on the reported IEP values. Moreover, detailed analyses of the bulk chemical compositions of natural materials used in IEP measurements are not available in most cases.

CONCLUSIONS AND IMPLICATIONS

In this study, the differences in IEP values between single crystals and powdered forms of hydrated α-Al_2O_3 and α-Fe_2O_3 have been discussed. Literature IEP values of powdered samples of α-Al_2O_3 and α-Fe_2O_3 have been tabulated and compared. The streaming potential measurements by electrokinetic analyzer on three single-crystal surfaces [α-Al_2O_3 (0001) and (1-102) and α-Fe_2O_3 (0001)] have confirmed the differences in IEP values for powdered vs. single-crystal α-Al_2O_3, and have shown clear evidence for such differences in the case of α-Fe_2O_3. Such differences have also been found in surface charge measurements of single-crystal and powdered forms of more soluble solids like fluorite (Fa et al., 2005). The presence of various types of surface sites, particularly defect sites on particles in polycrystalline (powdered) samples, may explain the surface charge discrepancies between the powders and the single-crystal counterparts studied here (see Franks and Meagher, 2003; Franks and Gan, 2007; Zhang et al., 2008). In particular, our model calculations suggest that differences in surface concentrations of singly coordinated surface groups play a decisive role in determining the IEPs and explaining the differences in IEP between single crystals and powders of hydrated Al- and Fe(III)-oxides. Modeling studies of the surface charging behavior of hematite single crystal surfaces by Venema et al. (1998), Zarzycki et al. (2011), and Lützenkirchen et al. (2015) also concluded that different types of reactive surface groups affect surface charging behavior.

The recent study of Lützenkirchen et al. (2015) on the relationship between measured IEP values and surface structure, as revealed by crystal truncation rod (CTR) diffraction and AFM measurements on single crystal α-Fe_2O_3 (0001) surfaces before and after aging in aqueous solution, showed significant changes in IEP values and surface structure with aging. The proposed two-domain structural model for the aged hematite (0001) surface likely represents an

intermediate structure between the fresh two-domain surface and a fully aged, one-domain (oxygen- or hydroxyl-terminated) surface (cf. Lützenkirchen et al., 2013). Lützenkirchen et al. (2015) interpreted their combined IEP and CTR results for fresh hematite (0001) as indicating a very flat, weakly hydrated surface. In contrast, they suggest that aged hematite (0001) shows an increase in *"hydration of the surface with time and enhanced reactivity of singly-coordinated hydroxyl groups that causes the isoelectric point of the surface to shift to values that are reminiscent of those typically reported for hematite particles."*

Modeling studies of IEP values of metal oxides based on estimated proton affinities and assuming certain concentrations of singly or multiply coordinated surface (hydr)oxo groups predict IEP values that deviate from those determined experimentally (e.g., Venema et al., 1998; Zarzycki and Preocanin, 2012; Chatman et al., 2013; Shimizu and Boily, 2014). A similar statement can be made concerning the difference in measured IEP values of single crystal surfaces and those predicted using the Sverjensky model based on bond valence and solvation theory (Sverjensky, 1994). These observations suggest that, in addition to surface defects, other factors affect IEP values, including long-range electrostatics that average site specificity (Zarzycki, 2007), differences in sample preparation methods and methods used for IEP determination (Lützenkirchen et al., 2015), differences in crystal morphologies (Venema et al., 1998), surface compositions (Franks and Gan, 2007), sample aging in aqueous solutions (Lützenkirchen et al., 2013, 2015), and possibly differences in particle size in the nanoparticle size range (Vayssieres, 2009 and Table 3).

Although an interesting new model for the IEP value of single-crystal α-Al_2O_3 (0001) based on auto-photolysis of interfacial water has been proposed by Lützenkirchen et al. (2010), we question the universal validity of the hydrophobicity of metal-oxide surfaces (Gentleman and

643 Ruud, 2010) assumed in this model based on recent high pressure XPS studies of the interaction
644 of water with single crystal metal-oxide surfaces such as MgO(100) (Newberg et al., 2011a;
645 Newberg et al., 2011b; Newberg, 2014) and α-Fe_2O_3(0001) (Yamamoto et al., 2010). These *in*
646 *situ* XPS studies show that surface hydroxylation can be correlated with the build-up of multiple
647 layers of molecular water on these surfaces.

648 The results of our modeling study parallel the earlier efforts of Venema et al. (1998) to
649 predict the proton affinity of reactive surface sites on the (001) and (110) surfaces of hematite
650 crystals based on potentiometric titrations and MUSIC modeling of proton affinities assuming a
651 structure for selected surface sites. However, in the present study we based our modeling on
652 measured average structure (Trainor et al., 2004) of the hydrated (0001) hematite surface and our
653 surface charging measurements were made on single crystals that were prepared in the same
654 manner as used in our earlier crystal truncation rod x-ray diffraction measurements (Trainor et
655 al., 2004). More systematic IEP studies of powdered samples of metal oxides of different sizes
656 and morphologies, but with well-characterized surface properties and compositions, are required
657 to verify if the IEP variations are caused by varying particle size (cf. Vayssieres, 2009; Ridley et
658 al., 2013). Our model calculations suggest, however, that increased concentrations of singly
659 coordinated surface groups on hydrated α-Al_2O_3 and α-Fe_2O_3 particle surfaces, which should
660 increase with decreasing particle size in the nanoparticle size range, should result in higher IEP
661 values.

662 The recent study of Lützenkirchen et al. (2015) found that an aged α-Fe_2O_3 (0001)
663 sample with an IEP value of 9 has less singly coordinated surface groups (32%) than the fresh α-
664 Fe_2O_3 (0001) sample with a dramatically lower IEP value of 4 (56%). Although this finding
665 appears to contradict our claim that an increase in singly coordinated surface groups results in a

666 higher IEP value, the singly coordinated surface groups on the aged α-Fe_2O_3 (0001) sample have
667 much shorter Fe-O distances and much more adsorbed and spatially ordered water than the fresh
668 samples. Based on these differences, Lützenkirchen et al. (2015) suggest that the much higher
669 reactivity of the singly coordinated surface groups of the aged sample causes the IEP of the aged
670 sample to be significantly higher.

671 Although single-crystal surfaces are not as relevant to natural systems as their
672 polycrystalline or nanocrystalline counterparts, they represent a base model system that allows us
673 to account for differences in average surface structure determined by crystal truncation rod
674 diffraction studies (Eng et al., 2000; Trainor et al., 2002, 2004; Tanwar et al., 2007). The
675 knowledge gained about the surface structures of single crystals can be used in explaining their
676 different reactivities to water and to metal ions and/or pollutant species. In contrast, detailed
677 surface structures of small particles, especially nanoparticles, have not been measured
678 experimentally as no experimental methods are yet available to provide structural details.

679 Differences in charging behavior of mineral surfaces caused by differences in structure
680 and/or composition, including the effects of microbial biofilm and/or natural organic matter
681 coatings, can have significant impacts on their electrostatic interactions with metal ions and/or
682 pollutant species. The surface charges of Fe- and Al-(oxyhydr)oxides are typically positive at
683 neutral pH, with IEP values in the range of 8-9 for polycrystalline powders and nanoparticles,
684 and in the range of 4-7 for single-crystal surfaces studied here (Parks, 1965; Sverjensky, 1994;
685 Franks and Meagher, 2003). In contrast, the surface charge of bacteria is negative in most cases
686 under neutral pH conditions (Yee et al., 2004). Therefore, bacteria and microbial biofilms can
687 potentially compete with mineral surfaces for metal-ion sorption and/or result in more negatively
688 charged mineral surfaces (Wang et al., in press). A better understanding of surface charge

properties is essential for predicting relative differences in metal-ion sorption behavior in complex systems such as microbe/metal-oxide/water systems.

ACKNOWLEDGMENTS

Financial support for this project was provided by NSF Grant CHE-0431425 (Stanford Environmental Molecular Science Institute) and by the NSF-Center for Environmental Implications for Nanotechnology (based at Duke University) (NSF Cooperative Agreement EF-0830093). One of us (P.P.) acknowledges financial support from the Swedish Research Council, the Wenner-Gren Foundations and the Blaustein Visiting Professorship Fund of the School of Earth, Energy, and Environmental Sciences, Stanford University. We thank Dr. Federico Pacheco and Dr. Sophie Walewijk for their help with steaming potential measurements. Prof. Stefan Sjoberg (Dept. of Chemistry, Umeå University, Sweden), Prof. Piotr Zarzycki (Institute of Physical Chemistry, Polish Academy of Sciences, Warsaw, Poland), and an anonymous referee are also thanked for their helpful comments, which improved the manuscript. Lastly, GEB wishes to thank his former Stanford colleague Prof. George A. Parks for many stimulating discussions about IEP values of metal oxides over the 25 years we overlapped at Stanford University and worked together on many research projects on interface chemistry and geochemistry.

REFERENCES

Avgouropoulos, G., Ioannides, T., Papadopoulou, C., Batista, J., Hocevar, S., and Matralis, H.K. (2002) A comparative study of Pt/γ-Al_2O_3, Au/α-Fe_2O_3 and CuO-CeO_2 catalysts for the selective oxidation of carbon monoxide in excess hydrogen. Catalysis Today, 75, 157-167.

Barr, T.L., and Seal, S. (1995) Nature of the use of adventitious carbon as a binding-energy standard. Journal of Vacuum Science and Technology A: Vacuum, Surfaces, and Films, 13, 1239-1246.

Bhargava, G., Gouzman, I., Chun, C.M., Ramanarayanan, T.A., and Bernasek, S.L. (2007) Characterization of the "native" surface thin film on pure polycrystalline iron: A high resolution XPS and TEM study. Applied Surface Science, 253, 4322-4329.

Brown Jr., G.E., Henrich, V.E., Casey, W.H., Clark, D.L., Eggleston, C., Felmy, A., Goodman, D. W., Gratzel, M., Maciel, G., McCarthy, M.I., Nealson, K.H., Sverjensky, D.A., Toney, M.F., and Zachara, J.M. (1999) Metal oxide surfaces and their interactions with aqueous solutions and microbial organisms. Chemical Reviews, 99, 77-174.

Chatman, S., Zarzycki, P., and Rosso, K. M. (2013) Surface potentials of (001), (012), (113) hematite (α-Fe_2O_3) crystal faces in aqueous solution. Physical Chemistry Chemical Physics, 15, 13911-13921.

Chibowski, S., Patkowski, J., and Opala-Mazur, E. (2005) Adsorption of commercial, filtrated and fractionated polyethylene oxide onto hematite. Materials Chemistry and Physics, 92, 519-525.

Chorover, J., and Sposito, G. (1995) Surface-charge characteristics of kaolinitic tropical soils. Geochimica et Cosmochimica Acta, 59, 875-884.

Christl, I., and Kretzschmar, R. (1999) Competitive sorption of copper and lead at the oxide-water interface: Implications for surface site density. Geochimica et Cosmochimica Acta, 63, 2929-2938.

Cornell R.M. and Schwertmann, U. (2003) The Iron Oxides: Structure, Properties, Reactions, Occurrences and Uses (2nd Ed.). Wiley-VCH GmbH & Co. KGaA, Weinheim, 664 p.

Eggleston, C.M., and Jordan, G. (1998) A new approach to pH of point of zero charge measurement: Crystal-face specificity by scanning force microscopy (SFM). Geochimica et Cosmochimica Acta, 62, 1919-1923.

El Badawy, A.M., Silva, R.G., Morris, B., Scheckel, K.G., Suidan, M.T., and Tolaymat, T.M. (2011) Surface charge-dependent toxicity of silver nanoparticles. Environmental Science & Technology, 45, 283-287.

Eng, P.J., Trainor, T.P., Brown Jr., G.E., Waychunas, G.A., Newville, M., Sutton, S.R., and Rivers, M.L. (2000) Structure of the hydrated α-Al_2O_3 (0001) surface. Science, 288, 1029-1033.

Fa, K.Q., Paruchuri, V.K., Brown, S.C., Moudgil, B.M., and Miller, J.D. (2005) The significance of electrokinetic characterization for interpreting interfacial phenomena at planar, macroscopic interfaces. Physical Chemistry Chemical Physics, 7, 678-684.

Fitts, J.P., Shang, X.M., Flynn, G.W., Heinz, T.F., and Eisenthal, K.B. (2005) Electrostatic surface charge at aqueous/α-Al_2O_3 single-crystal interfaces as probed by optical second-harmonic generation. Journal of Physical Chemistry B, 109, 7981-7986.

Franks, G.V., and Gan, Y. (2007) Charging behavior at the alumina-water interface and implications for ceramic processing. Journal of American Ceramic Society, 90, 3373-3388.

Franks, G.V., and Lange, F.F. (1999) Mechanical behavior of saturated, consolidated, alumina powder compacts: Effect of particle size and morphology on the plastic-to-brittle transition. Colloids and Surface A: Physicochemical and Engineering Aspects, 146, 5-17.

Franks, G.V., and Meagher, L. (2003) The isoelectric points of sapphire crystals and α-alumina powder. Colloids and Surfaces A: Physicochemical and Engineering Aspects, 214, 99-110.

Gentleman, M.M., and Ruud, J.A. (2010) Role of hydroxyls in oxide wettability. *Langmuir*, 26, 1408-1411.

Gibbs, R.J. (1983) Effect of natural organic coatings on the coagulation of particles. Environmental Science & Technology, 17, 237-240.

761 Goldberg, S., Davis, J.A., and Hem, J.D. (1996) The surface chemistry of aluminum oxides and
762 hydroxides. In: The Environmental Chemistry of Aluminum, 2nd Ed. (G. Sposito Ed.), CRC
763 Lewis Publishers, Boca Raton, pp. 271-331.
764 Gu, B., Mehlhorn, T.L., Liang, L., and McCarthy, J.F. (1996) Competitive adsorption,
765 displacement, and transport of organic matter on iron oxide: I. Competitive adsorption.
766 Geochimica et Cosmochimica Acta, 60, 1943-1950.
767 Gunnarsson, M., Rasmusson, M., Wall, S., Ahlberg, E., and Ennis, J. (2001) Electroacoustic and
768 potentiometric studies of the hematite/water interface. Journal of Colloid & Interface Science,
769 240, 448-458.
770 Hiemstra, T., van Riemsdijk, W.H., and Bolt, G.H. (1989) Multisite proton adsorption modeling
771 at the solid-solution interface of (hydr)oxides - a new approach: 1. Model description and
772 evaluation of intrinsic reaction constants. Journal of Colloid & Interface Science, 133, 91-
773 104.
774 Hizal, J., Apak, R., and Hoell, W.H. (2009) Modeling competitive adsorption of copper(II),
775 lead(II), and cadmium(II) by kaolinite-based clay mineral/humic acid system. Environmental
776 Progress & Sustainable Energy, 28, 493-506.
777 Honeyman, B.D., and Santschi, P.H. (1991) Coupling adsorption and particle aggregation -
778 laboratory studies of colloidal pumping using Fe-59 labeled hematite. Environmental Science
779 & Technology, 25, 1739-1747.
780 Jeon, B.H., Dempsey, B.A., Burgos, W.D., and Royer, R.A. (2001) Reactions of ferrous iron
781 with hematite. Colloids and Surface A: Physicochemical and Engineering Aspects, 191, 41-
782 55.
783 Kershner, R.J., Bullard, J.W., and Cima, M.J. (2004) Zeta potential orientation dependence of
784 sapphire substrates. Langmuir, 20, 4101-4108.
785 Kim, E. K., and Walker, H. W. (2001) Effect of cationic polymer additives on the adsorption of
786 humic acid onto iron oxide particles. Colloids and Surface A: Physicochemical and
787 Engineering Aspects, 194, 123-131.
788 Kirwan, L.J., Fawell, P.D., and van Bronswijk, W. (2004) An in situ FTIR-ATR study of
789 polyacrylate adsorbed onto hematite at high pH and high ionic strength. Langmuir, 20, 4093-
790 4100.
791 Kosmulski, M. (2001). Chemical Properties of Material Surfaces. Dekker, New York.
792 Kosmulski, M. (2004) pH-dependent surface charging and points of zero charge - II. Update.
793 Journal of Colloid & Interface Science, 275, 214-224.
794 Kosmulski, M. (2006) pH-dependent surface charging and points of zero charge III. Update.
795 Journal of Colloid & Interface Science, 298, 730-741.
796 Kosmulski, M. (2009a) Compilation of PZC and IEP of sparingly soluble metal oxides and
797 hydroxides from literature. Advances in Colloid & Interface Science, 152, 14-25.
798 Kosmulski, M. (2009b) pH-dependent surface charging and points of zero charge. IV. Update
799 and new approach. Journal of Colloid & Interface Science, 337, 439-448.
800 Kosmulski, M. (2009c) Surface Charging and Points of Zero Charge, Surfactant Science Series,
801 vol. 145. CRC Press, Taylor & Francis Group, LLC, Boca Raton, FL.
802 Larson, I., Drummond, C.J., Chan, D.Y.C., and Grieser, F. (1997) Direct force measurements
803 between silica and alumina. Langmuir, 13, 2109-2112.
804 Liu, P., Kendelewicz, T., and Brown Jr., G.E. (1998) Reaction of water with MgO(100) surfaces.
805 Part II: Synchrotron photoemission studies of defective surfaces. Surface Science, 412-13,
806 315-332.

Loaec, M., Olier, R., and Guezennec, J. (1997) Uptake of lead, cadmium and zinc by a novel bacterial exopolysaccharide. Water Research, 31, 1171-1179.

Lützenkirchen, J., Heberling, F., Supljika, F., Preocanin, T., Kallay, N., Johann, F., Weisser, L., and Eng, P. (2015) Structure-charge relationship - the case of hematite (001). Faraday Discussions, 180, 55-79.

Lützenkirchen, J., Preocanin, T., Stipic, F., Heberling, F., Rosenqvist, J., and Kallay, N. (2013) Surface potential at the hematite (001) crystal lane and the effects of prolonged aging in water. Geochimica et Cosmochimica Acta, 120, 479-486.

Lützenkirchen, J., Zimmermann, R., Preocanin, T., Filby, A., Kupcik, T., Kuttner, D., Abdelmonem, A., Schild, D., Rabung, T., Plaschke, M., Brandenstein, F., Werner, C., and Geckeis, H. (2010) An attempt to explain bimodal behaviour of the sapphire c-plane electrolyte interface. Advances in Colloid and Interface Science, 157, 61-74.

Mayer, L.M. (1999) Extent of coverage of mineral surfaces by organic matter in marine sediments. Geochimica et Cosmochimica Acta, 63, 207-215.

Miller, D.J., Biesinger, M.C., and McIntyre, N.S. (2002) Interactions of CO_2 and CO at fractional atmosphere pressures with iron and iron oxide surfaces: one possible mechanism for surface contamination? Surface and Interface Analysis, 33, 299-305.

Newberg, J.T. (2014) Surface thermodynamics and kinetics of MgO(100) terrace site hydroxylation. Journal of Physical Chemistry C, 118, 29187-29195.

Newberg, J.T., Starr, D.E., Yamamoto, S., Kaya, S., Kendelewicz, T., Mysak, E.R., Porsgaard, S., Salmeron, M.B., Brown Jr., G.E., Nilsson, A., and Bluhm, H. (2011a) Formation of hydroxyl and water layers on MgO films studied with ambient pressure XPS. Surface Science, 605, 89-94.

Newberg, J.T., Starr, D.E., Yamamoto, S., Kaya, S., Kendelewicz, T., Mysak, E.R., Porsgaard, S., Salmeron, M.B., Brown Jr., G.E., Nisson, A., and Bluhm, H. (2011b) Autocatalytic surface hydroxylation of MgO(100) terrace sites observed under ambient conditions. Journal of Physical Chemistry C, 115, 12864-12872.

Nordin, J., Persson, P., Nordin, A., and Sjoberg, S. (1998) Inner-sphere and outer-sphere complexation of a polycarboxylic acid at the water-boehmite (γ-AlOOH) interface: A combined potentiometric and IR spectroscopic study. Langmuir, 14, 3655-3662.

Olefjord, I., and Nylund, A. (1994) Surface-analysis of oxidized aluminum 2. Oxidation of aluminum in dry and humid atmosphere studied by ESCA, SEM, SAM and EDX. Surface and Interface Analysis, 21, 290-297.

Pan, Z.H., Somasundaran, P., Turro, N.J., and Jockusch, S. (2004) Interactions of cationic dendrimers with hematite mineral. Colloids and Surface A: Physicochemical and Engineering Aspects, 238, 123-126.

Parks, G.A. (1965) Isoelectric points of solid oxides solid hydroxides and aqueous hydroxo complex systems. Chemical Review, 65, 177-198.

Ridley, M.K., Machesky, M.L. and Kubicki, J.D. (2013) Anatase nanoparticle surface reactivity in NaCl media: A CD-Music model interpretation of combined experimental and density functional theory studies. Langmuir, 29 (27), 8572-8583.

Shimizu, K. and Boily, J.-F. (2014) Electrochemical properties and relaxation times of the hematite/water interface. Langmuir, 30 (31), 9591-9598.

Sposito, G. (1984) The Surface Chemistry of Soils. Oxford University Press, Inc., 234pp.

Stack, A.G., Higgins S.R., and Eggleston C.M. (2001) Point of zero charge of a corundum-water interface probed with optical second harmonic generation (SHG) and atomic force

microscopy (AFM): New approaches to oxide surface charge. Geochimica et Cosmochimica Acta, 65, 3055-3063.

Stipp, S.L.S., Hansen, M., Kristensen, R., Hochella Jr., M.F., Bennedsen, L., Dideriksen, K., Balic-Zunic, T., Leonard, D., and Mathieu, H.J. (2002) Behaviour of Fe-oxides relevant to contaminant uptake in the environment. Chemical Geology, 190, 321-337.

Sverjensky, D.A. (1994) Zero-point-of-charge prediction from crystal-chemistry and solvation theory. Geochimica et Cosmochimica Acta, 58, 3123-3129.

Tanwar, K.S., Lo, C.S., Eng, P. J., Catalano, J.G., Walko, D.A., Brown Jr., G.E., Waychunas, G.A., Chaka A.M., and Trainor T.P. (2007) Surface diffraction study of the hydrated hematite (1-102) surface. Surface Science, 601, 460-474.

Trainor, T.P., Chaka, A.M., Eng, P.J., Newville, M., Waychunas, G.A., Catalano, J.G. and Brown Jr., G.E. (2004) Structure and reactivity of the hydrated hematite (0001) surface. Surface Science, 573, 204-224.

Trainor, T.P., Eng, P.J., Brown Jr., G.E., Robinson, I. K., and De Santis, M. (2002) Crystal truncation rod diffraction study of the α-Al_2O_3 (1-102) surface. Surface Science, 496, 238-250.

Tulpar, A., Henderson, D.B., Mao, M., Caba, B., Davis, R.M., van Cott, K.E., and Ducker, W. A. (2005) Unnatural proteins for the control of surface forces. Langmuir, 21, 1497-1506.

Vayssieres, L. (2009) On the effect of nanoparticle size on water-oxide interfacial chemistry. Journal of Physical Chemistry C, 113, 4733-4736.

Veeramasuneni, S., Yalamanchili, M.R., and Miller, J.D. (1996) Measurement of interaction forces between silica and α-alumina by atomic force microscopy. Journal of Colloid & Interface Science, 184, 594-600.

Venema, P., Hiemstra, T., Weidler, P.G., and van Riemsdijk, W.H. (1998) Intrinsic proton affinity of reactive surface groups of metal (hydr)oxides: Application to iron (hydr)oxides. Journal of Colloid & Interface Science, 198, 282-295.

Wang, Y., Gélabert, A., Michel, F.M., Choi, Y., Gescher, J., Ona-Nguema, G., Eng, P.J., Bargar, J.R., Ghose, S., Farges, F., Spormann, A.M., and Brown, Jr., G.E. (in press) Partitioning of trace metals at biofilm/mineral/water interfaces: Part I: Impact of *Shewanella oneidensis* MR-1 biofilm coating on Pb(II) and Zn(II) partitioning and speciation at α-Al_2O_3/water and α-Fe_2O_3/water interfaces. Geochimica et Cosmochimica Acta.

Weiss, W., and Ranke, W. (2002) Surface chemistry and catalysis on well-defined epitaxial iron-oxide layers. Progress in Surface Science, 70, 1-151.

Wightman, P.G., and Fein, J.B. (2001) Ternary interactions in a humic acid-Cd-bacteria system. Chemical Geology, 180, 55-65.

Yamamoto, S., Kendelewicz, T., Newberg, J.T., Ketteler, G., Starr, D.E., Mysak, E.R., Andersson, K.J., Ogasawara, H., Bluhm, H., Salmeron, M., Brown Jr., G.E., and Nilsson A. (2010) Water adsorption on α-Fe_2O_3(0001) at near ambient conditions. Journal of Physical Chemistry C, 114, 2256-2266.

Yang, Q.Z., and Troczynski, T. (1999) Dispersion of alumina and silicon carbide powders in alumina sol. Journal of American Ceramic Society, 82, 1928-1930.

Yee, N., Fowle, D.A., and Ferris F. G. (2004) A Donnan potential model for metal sorption onto *Bacillus subtilis*. Geochimica et Cosmochimica Acta, 68, 3657-3664.

Zarzycki, P. (2007) Effective adsorption energy distribution function as a new mean-field characteristic of surface heterogeneity in adsorption systems with lateral interactions. Journal of Colloid & Interface Science, 311, 622-627.

Zarzycki, P., Chatman, S., Preocanin, T., and Rosso, K.M. (2011) Electrostatic potential of specific mineral faces. Langmuir, 27, 7986-7990.

Zarzycki, P. and Preocanin, T. (2012) Point of zero potential of single-crystal electrode/inert electrolyte interface. Journal of Colloid & Interface Science, 370, 139-143.

Zhang L., Tian C., Waychunas, G.A., and Shen Y.R. (2008) Structures and charging of α-alumina (0001)/water interfaces studied by sum-frequency vibrational spectroscopy. Journal of the American Chemical Society, 130, 7686-7694.

908 **Table 1:** Isoelectric point (IEP) values of single-crystal α-Al_2O_3 (0001), α-Al_2O_3 (1-102), and α-
909 Fe_2O_3 (0001) surfaces.
910

Surface	Methods	IEP	References
α-Al_2O_3 (0001)	Streaming potential and AFM	4.2	Larson et al., 1997
α-Al_2O_3 (0001)	Second harmonic generation and AFM	4.8-5.4	Stack et al., 2001
α-Al_2O_3 (0001)	Streaming potential and AFM	5.0	Franks and Meagher, 2003
α-Al_2O_3 (0001)	Second harmonic generation	4.1	Fitts et al., 2005
α-Al_2O_3 (0001)	Sum-frequency vibrational spectroscopy	6.3 (±1.2)	Zhang et al., 2008
α-Al_2O_3, orientation not specified	AFM (plasma treated)	9.3	Veeramasuneni et al., 1996
α-Al_2O_3 (0001)	AFM (plasma treated)	8.5	Tulpar et al., 2005
α-Al_2O_3 (0001)	AFM (without plasma treatment)	5-6	Tulpar et al., 2005
α-Al_2O_3 (0001)	Streaming potential	4	Lützenkirchen et al., 2010
α-Al_2O_3 (0001)	Streaming potential	4.5	This study
α-Al_2O_3 (1-102)	Streaming potential and AFM	5.85	Franks and Meagher, 2003
α-Al_2O_3 (1-102)	Second harmonic generation	5.2 (±0.4)	Fitts et al., 2005
α-Al_2O_3 (1-102)	Streaming potential	5.1	This study
α-Fe_2O_3 (0001)	Streaming potential	6.5	This study
α-Fe_2O_3 (0001)	Scanning force microscopy	8-8.5	Eggleston and Jordon, 1998
α-Fe_2O_3 (0001)	SCrE Cyclic Potentiometry	8	Zarzycki et al., 2011
α-Fe_2O_3 (0001)	SCrE Cyclic Potentiometry	8.1-8.4	Lützenkirchen et al., 2013
α-Fe_2O_3 (0001)	SCrE Cyclic Potentiometry	8.35	Chatman et al., 2013
α-Fe_2O_3 (0001)	SCrE Cyclic Potentiometry and Zeta potential	4-9	Lützenkirchen et al., 2015

911
912

This is a preprint, the final version is subject to change, of the American Mineralogist (MSA)
Cite as Authors (Year) Title. American Mineralogist, in press.
(DOI will not work until issue is live.) DOI: http://dx.doi.org/10.2138/am-2016-5531

Table 2: Compositions and pK_a values of surface functional groups on single-crystal α-Al_2O_3 (0001) and (1-102) and α-Fe_2O_3 (0001) surfaces.

Surface group	α-Al_2O_3 (0001)		α-Al_2O_3 (1-102)		α-Fe_2O_3 (0001)	
	Present[#]	pK_a*	Present[#]	pK_a*	Present[#]	pK_a*
$(Me)OH_2^{+0.5}$	No		Yes	10.0	Yes	10.6
$(Me)_2OH_2^{+1.0}$	Yes	-1.5	Yes	-1.5	Yes	-0.2
$(Me)_2OH$	Yes	12.3	Yes	12.3	Yes	13.6
$(Me)_3OH^{+0.5}$	No		Yes	2.2	Yes	4.3

*pK_a values estimated using the classical MUSIC model (Hiemstra et al., 1989; Venema et al., 1998).

[#]Predominant surface functional group based on previous CTR diffraction studies (Eng et al., 2000; Trainor et al. 2002; Trainor et al., 2004; Tanwar et al., 2007).

Table 3: Isoelectric point (IEP) or point of zero charge (PZC) of hematite polycrystalline powders with known surface properties. SSA = specific surface area, D_{avg} = average particle diameter.

Surface	Methods and Experimental Conditions	IEP	References
α-Fe_2O_3, synthetic from chloride	Spherical, SSA=4.6 m^2g^{-1}, D_{avg}=250nm, IEPs by coagulation and titration methods	8.6	Honeyman and Santschi, 1991
α-Fe_2O_3, synthetic from chloride	D_{avg}=77±3nm, 10^{-3} mol dm^{-3} KCl, IEPs by classical electrokinetic methods	9.2	Zhang and Buffle, 1995
α-Fe_2O_3, synthetic from chloride	Matijevic and Scheiner's methods, SSA=16.7m^2g^{-1}, D_{avg}=100nm, spherical uniform particles, 0.01–1 mol dm^{-3} $NaNO_3$, T=25°C, IEPs by titration at cip and by Acusto	9	Gunnarsson et al., 2001
α-Fe_2O_3, 99.9%, Atlantic Equipment Engineers	D_{avg}=307±18.5nm, 10^{-3} mol dm^{-3} NaCl, T=25°C, IEPs by classical electrokinetic methods	8.8	Kim and Walker, 2001
α-Fe_2O_3, synthetic, J.T. Baker	D_{avg}=1000nm, SSA=9.04 m^2g^{-1}, washed, 0.1N NaOH 24h, DDW, 0.1N HCl 24h, then DDW, 11 times, 0.001–0.1 mol dm^{-3} NaCl, IEPs by classical electrokinetic methods and by titration	8.5/8.5	Jeon et al., 2001
α-Fe_2O_3, Alfa Aesar	SSA=8.4 m^2g^{-1}, D_{avg} ~ 5 μm, 0.03 mol dm^{-3} NaCl, IEPs by classic electrokinetic methods (Zeta-Meter 3.0) and by acousto (DT-1200 Acoustic and Electroacoustic spectrometer)	6.5	Pan et al., 2004
α-Fe_2O_3, synthetic from $FeCl_3$	Monodispersed, D_{50}=96nm, T=23°C, IEPs by classic electrokinetic methods (Brookhaven ZetaPlus instrument)	10	Kirwan et al., 2004
α-Fe_2O_3, synthetic from $FeCl_3$	By Matijevic and Scheiner's methods, SSA=20.75m^2g^{-1}, D_{avg}=198.7nm, 0.01 mol dm^{-3} NaCl, T=25°C, IEPs by Malvern Zetasizer 3000	8.5	Chibowski et al., 2005
α-Fe_2O_3, synthetic from $FeCl_3$	SSA=28.3 ± 0.7m^2g^{-1}, D_{avg}=119 ± 29nm, spherical particles, 0.005–0.5 mol dm^{-3} $NaNO_3$, IEPs by titration at cip	9.5	Christl and Kretzschmar, 1999

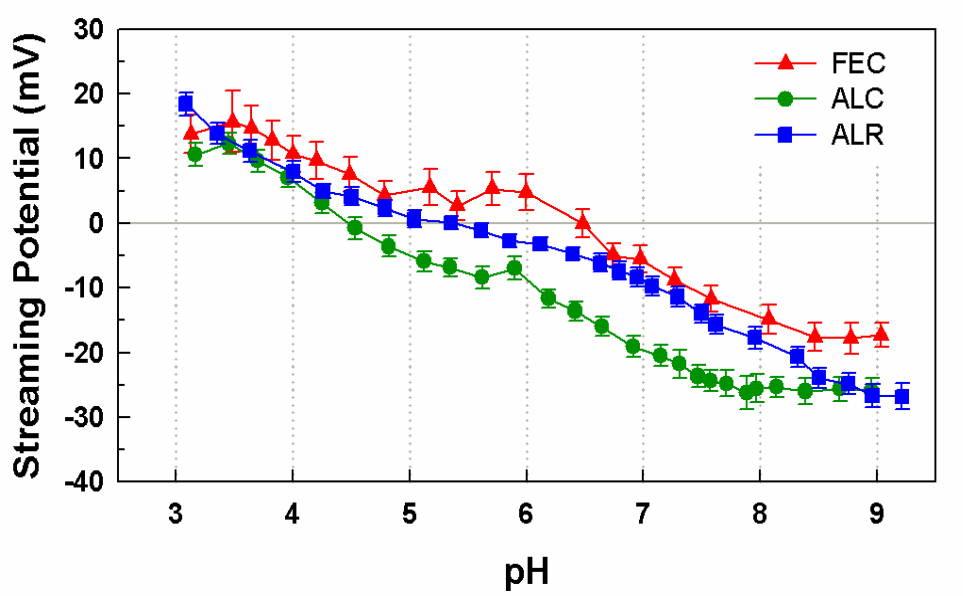

Figure 1. Streaming potential values as a function of pH for three metal-oxide single-crystal surfaces: FEC is the α-Fe_2O_3 (0001) surface, ALR is the α-Al_2O_3 (1-102) surface, and ALC is the α-Al_2O_3 (0001) surface.

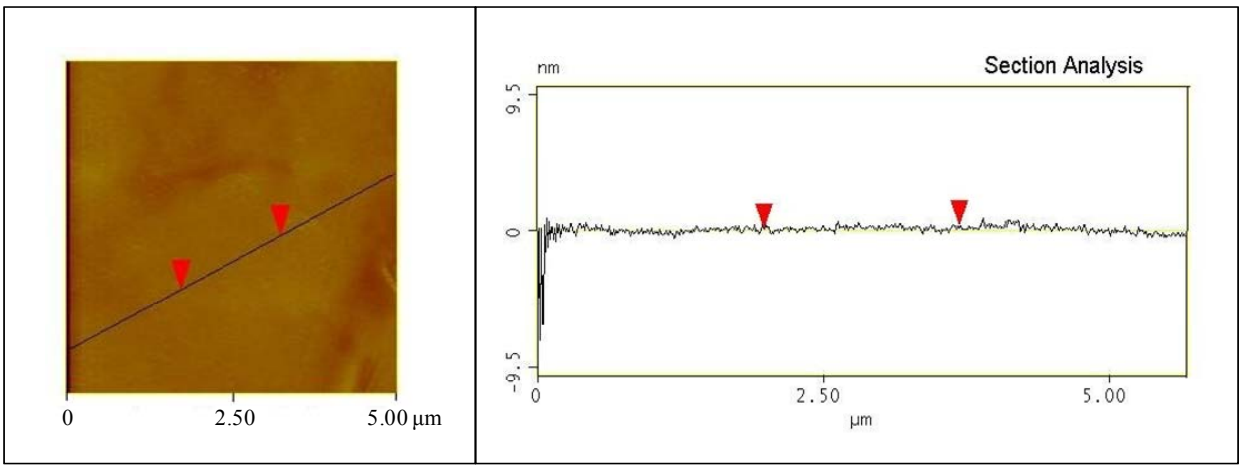

Figure 2a. (Left) Atomic force microscopy (AFM) image of the α-Fe_2O_3 (0001) surface after chemical-mechanical polishing and before streaming potential measurements. (Right) Roughness profile measured by AFM along the traverse shown in the image to the left.

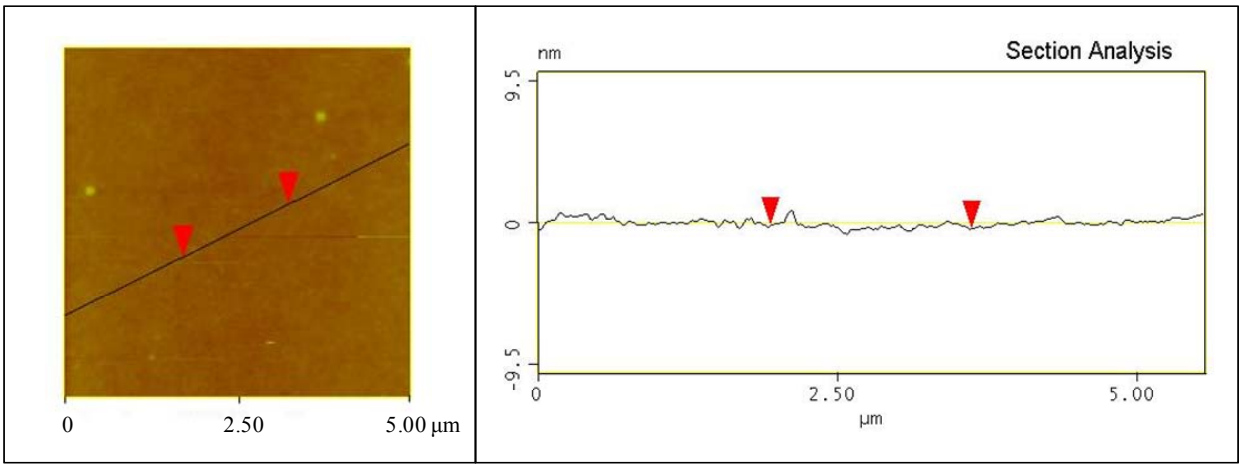

Figure 2b. (Left) Atomic force microscopy (AFM) image of the α-Al_2O_3 (0001) surface after chemical-mechanical polishing and before streaming potential measurements. (Right) Roughness profile measured by AFM along the traverse shown in the image to the left.

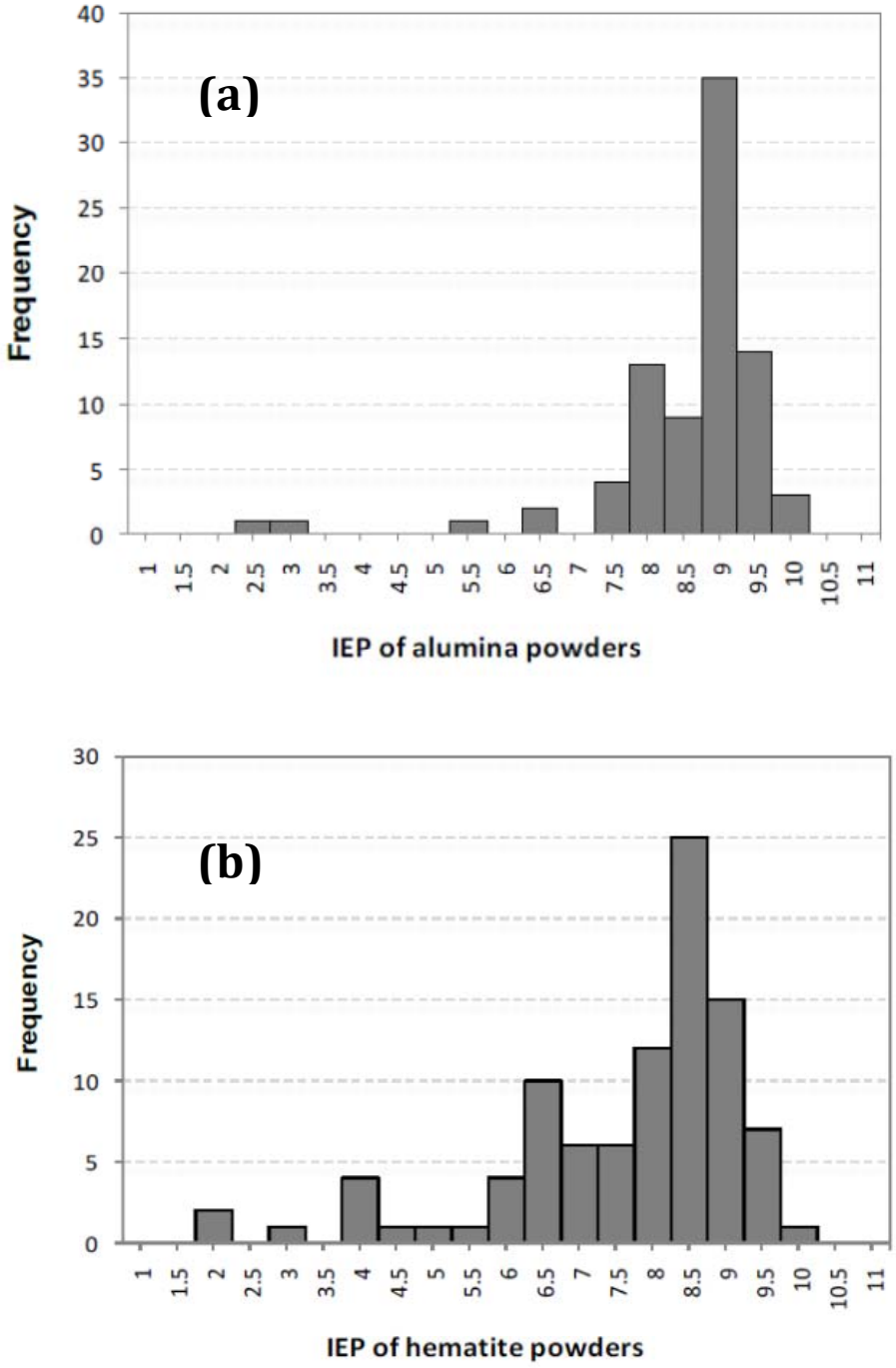

Figure 3. (a) Distribution of measured IEP values of alumina polycrystalline powders reported in the literature (total of 83 references – see Kosmulski, 2001, 2004, 2006, 2009a, 2009b, 2009c for references). **(b)** Distribution of measured IEP values of hydrated hematite powders in the literature (total of 96 references – see Kosmulski, 2001, 2004, 2006, 2009a, 2009b, 2009c for references).

1003

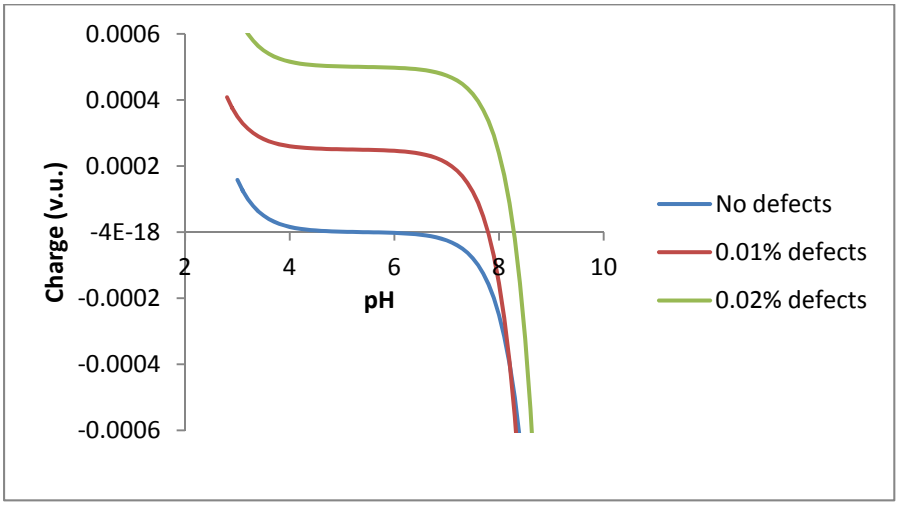

1004

1005 **Figure 4.** Simulation of surface charge (valence units expressed as μmol/m^2) of the α-Al_2O_3
1006 (0001) surface as a function of pH. Total concentration of doubly coordinated groups = 5
1007 μmol/m^2. Defects were assumed to be singly coordinated groups with concentrations expressed
1008 as percentage of the total concentration of the doubly coordinated groups. The pK_a values used in
1009 the calculations are listed in Table 2, and no electrostatic model was applied
1010

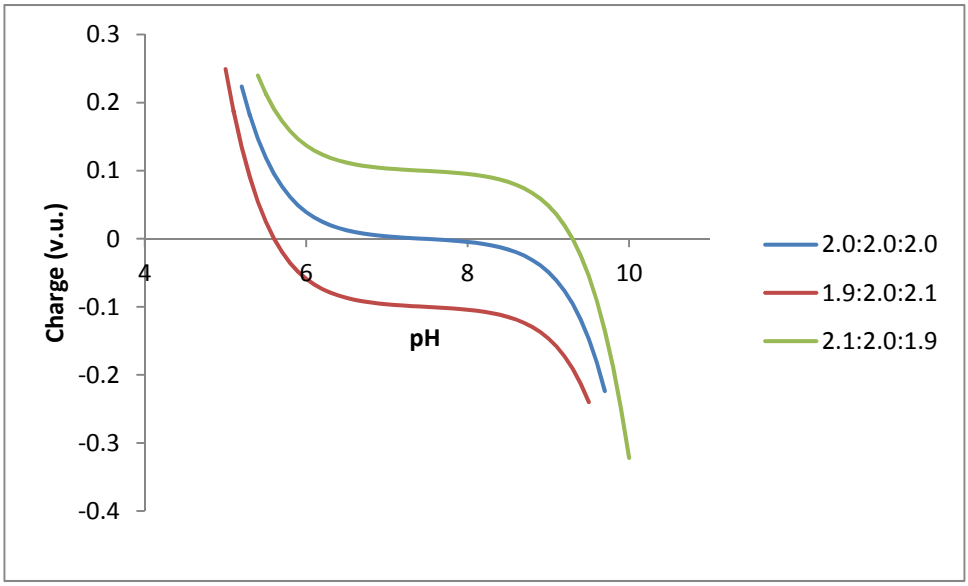

1011

1012 **Figure 5.** Simulation of surface charge (valence units expressed as μmol/m^2) of the α-Fe_2O_3
1013 (0001) surface as a function of pH. The legends denote the concentrations in μmol/m^2 of singly,
1014 doubly, and triply coordinated surface groups, respectively. The pK_a values used in the
1015 calculations are listed in Table 2 and no electrostatic model was applied.
1016